Senolytic Intervention Improves Cognition, Metabolism, and Adiposity in Female APP$^{NL-F/NL-F}$ Mice.

Yimin Fang[1], Mackenzie R. Peck[1], Kathleen Quinn[1], David Medina[2], Stephen Roy[1], Samuel A. McFadden[1], Andrzej Bartke[2,3], Kevin N. Hascup[1,3,4], *Erin R. Hascup[1,4]

[1]Department of Neurology, Dale and Deborah Smith Center for Alzheimer's Research and Treatment, Neuroscience Institute, Southern Illinois University School of Medicine, Springfield, IL 62702, USA.

[2]Department of Internal Medicine, Southern Illinois University School of Medicine, Springfield, IL 62702, USA.

[3]Department of Medical Microbiology, Immunology and Cell Biology, Southern Illinois University School of Medicine, Springfield, IL 62702, USA.

[4]Department of Pharmacology, Southern Illinois University School of Medicine, Springfield, IL 62702, USA.

*Corresponding Author: Erin R. Hascup, Department of Neurology, Dale and Deborah Smith Center for Alzheimer's Research and Treatment, Southern Illinois University School of Medicine, Springfield, IL 62794-9268, USA Tel: 217-545-6988, Email: ehascup@siumed.edu

Abstract

INTRODUCTION: Senescent cells accumulate throughout the body and brain contributing to unhealthy aging and Alzheimer's disease (AD). We hypothesized that senolytic intervention would alleviate cellular senescence thereby improving spatial memory in $APP^{NL\text{-}F/NL\text{-}F}$ mice.

METHODS: Male and female $APP^{NL\text{-}F/NL\text{-}F}$ mice were treated monthly with vehicle, 5 mg/kg Dasitinib (D) + 50 mg/kg Quercetin (Q), or 100 mg/kg Fisetin. Blood glucose levels, energy metabolism, spatial memory, and senescent cell markers were assayed.

RESULTS: D+Q treatment in female $APP^{NL\text{-}F/NL\text{-}F}$ mice increased oxygen consumption and energy expenditure resulting in decreased body mass. White adipose tissue content was decreased along with senescence markers, SASP, blood glucose, and plasma insulin and triglycerides. Hippocampal senescence markers and SASP were reduced along with soluble and insoluble $A\beta_{42}$ and SA-β-gal activity leading to improved spatial memory.

DISCUSSION: Considering women have a greater risk of dementia, identifying senotherapeutics appropriate for sex and disease stage is necessary for personalized medicine.

Key words: Quercetin, Fisetin, sexual dimorphism, senescent cells, Alzheimer's disease, senotherapeutics, white adipose tissue,

Research in Context

Systematic review: PubMed and Google Scholar were used to conduct literature reviews. Previous publications have shown senolytics improve cognition in tau and amyloid AD models. However, these studies were conducted at later disease stages when pathology was pronounced, do not examine effects in non-neuronal cell types, nor consider sex as a biological variable. We hypothesized senolytics could be used as a primary prevention against AD.

Interpretation: Our findings indicate Dasitinib plus Quercetin intervention acts in a sexually dimorphic manner that benefits female $APP^{NL\text{-}F/NL\text{-}F}$ mice when administered before overt signs of cognitive decline.

Future directions: The manuscript proposes a framework for the generation of new hypotheses and the conduct of additional studies. Examples include further understanding: (a) the lack of Dastinib + Quercetin efficacy in male $APP^{NL\text{-}F/NL\text{-}F}$ mice; (b) sex-dependent factors that contribute to adiposity changes after senolytic administration; and (c) changes in estrogen across the AD continuum and its potential role in modulating senolytic treatment.

Graphical Abstract

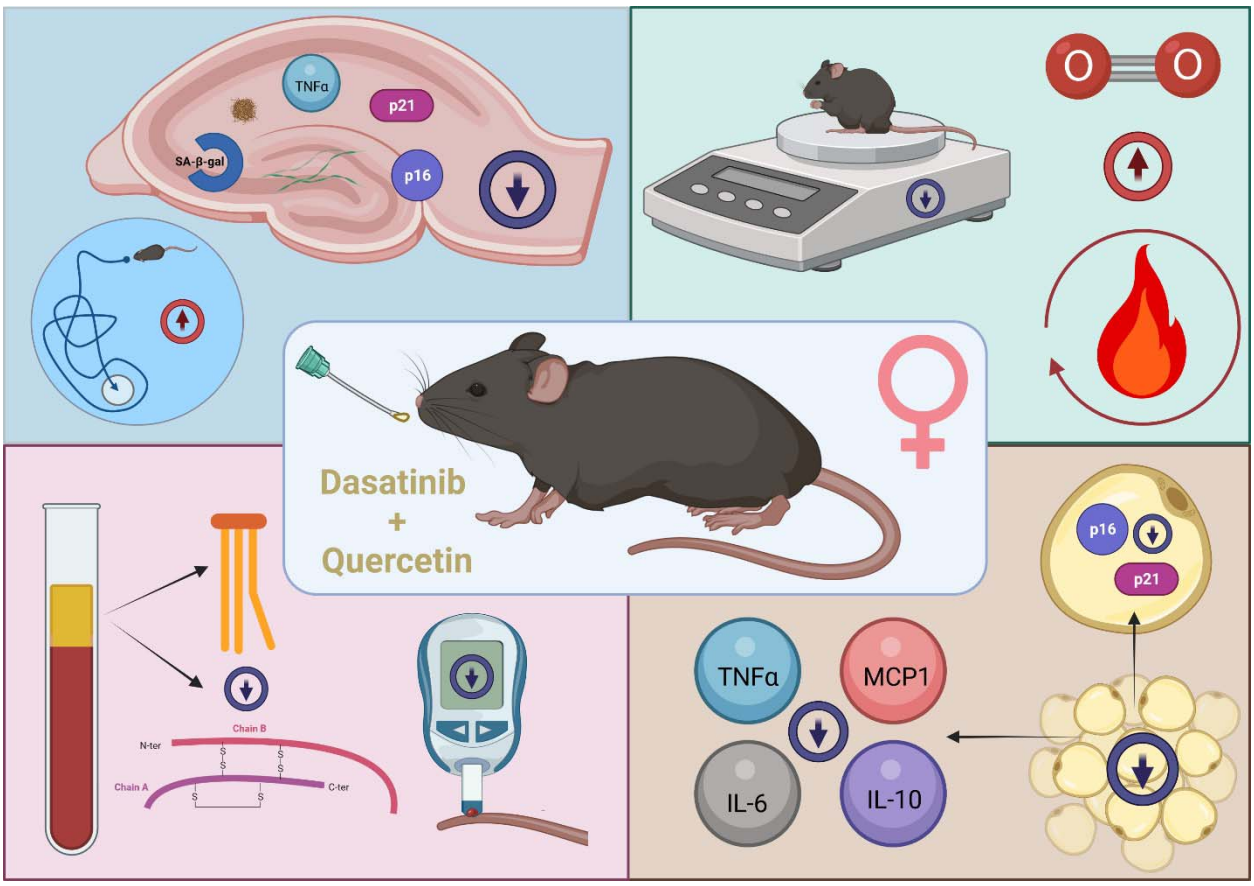

Monthly Dasatinib plus Quercetin administration in female $APP^{NL-F/NL-F}$ mice, but not males, led to improvements in multiple physiological parameters including increased oxygen consumption and energy expenditure resulting in decreased body mass. White adipose tissue content was decreased along with senescence markers, SASP, blood glucose, and plasma insulin and triglyceride levels. In the brain senescence markers and SASP were reduced along with soluble and insoluble $A\beta_{42}$ and SA-β-gal activity leading to improved spatial learning.

Introduction

The most prevalent form of dementia, Alzheimer's disease (AD), is an age-related neurodegenerative disorder that is considered the 6th leading cause of death in the United States. Nearly 6 million individuals living in the United States are estimated to have an AD diagnosis, and this number is expected to double every five years. The pathological hallmarks of AD are senile plaques composed of aggregated amyloid beta (Aβ) and neurofibrillary tangles formed from hyperphosphorylated tau protein. Approved therapies are limited, with those targeting cholinergic and glutamatergic signaling only providing symptomatic relief. Recent anti-amyloid antibodies show modest abatement of cognitive decline, but have edema and microhemorrhage risks [1]. This has prompted the field to continue searching for alternative therapeutic targets.

Numerous research efforts have explored the pathophysiology and treatment of AD. Separate gene mutations causing familial AD and preventing sporadic AD, gave rise to the amyloid cascade hypothesis [2] that has become a centralized dogma underlying AD research for several decades [3]. This has led to an incomplete understanding of causal pathways and slowing progress in the discovery of novel treatments [4]. Currently, AD is considered a multifactorial disease involving tau hyperphosphorylation, Aβ accumulation, inflammation, mitochondrial dysfunction, oxidative stress, and dysregulated cellular communication culminating in neuronal loss [5]. Cellular senescence, as a fundamental contributor to both aging and AD [6-8], is defined as cell cycle arrest governed by complex interactions across p21 and p16 tumor suppressive

Abbreviations: Alzheimer's disease (AD), Amyloid beta (Aβ), area under the curve (AUC), body weight (bw), brown adipose tissue (BAT), carbon dioxide consumption (VCO_2), corrected integrated path length (CIPL), Dasatinib (D), energy expenditure (EE), glucose tolerance test (GTT), insulin tolerance test (ITT), intraperitoneal (i.p.), Morris water maze (MWM), oxygen consumption (VO_2), Quercetin (Q), respiratory quotient (RQ), senescence-associated-β-galactosidase (SA-β-gal), senescence associated secretory phenotype (SASP), standard error of the mean (SEM), white adipose tissue (WAT), visceral white adipose tissue (vWAT)

pathways [9]. Senescent cells accumulate in nearly every tissue type of the body including the brain [10]. Their accumulation drives the production of senescent markers including p21, p16, and SASP [8, 11], which is involved in the expression of inflammatory cytokines, chemokines, growth factors, and matrix remodeling factors [12]. Over time the SASP profile can affect neighboring cells leading to a vicious cycle of cellular dysfunction.

Genetic deletion of senescent cells from the brain or treatment with senolytic drugs such as navitoclax [13], D+Q [14, 15], or Q [16, 17] has led to functional improvements in several different tau and amyloid AD models. The majority of these studies were conducted at later disease stages when pathology was pronounced. We hypothesized senolytics could be used as a primary prevention against AD. To test our hypothesis, we utilized a knock-in mouse model of AD ($APP^{NL\text{-}F/NL\text{-}F}$) carrying the Swedish (NL) and Beyreuther/Iberian (F) mutations [18, 19] that slowly develop plaque pathology starting at six months of age. From 4 to 13 months of age, male and female $APP^{NL\text{-}F/NL\text{-}F}$ mice were treated monthly with either 5 mg/kg D + 50 mg/kg Q or 100 mg/kg Fisetin similar to our previous protocols [20]. The results revealed that treatment with D+Q improved cognitive function accompanied with reduced senolytic markers in the brain and adipose tissue and other physiological parameters in female $APP^{NL\text{-}F/NL\text{-}F}$ mice.

Results

D+Q treatment decreases body weight via reduced adiposity in female $APP^{NL\text{-}F/NL\text{-}F}$ mice

Metabolic deficits leading to increased oxidative stress has been observed in AD patients and transgenic mouse models prior to plaque and tangle development [21-23]. In the $APP^{NL-F/NL-F}$ mice, Aβ deposition begins at 6 months of age with cognitive impairments occurring at 12-18 months [18]. To examine the metabolic changes associated with senolytic administration, body composition, glucose utilization, and energy metabolism were measured. When compared to control treatment, D+Q decreased body weight while an increase was observed in Fisetin-treated female $APP^{NL-F/NL-F}$ mice. Male $APP^{NL-F/NL-F}$ mice had no change in body weight with either senolytic treatment (Fig. 1A). We examined body composition of brown and white adipose tissue (BAT; WAT) depots to determine changes from senolytic administration. The percentages of total WAT consisting of subcutaneous WAT, visceral (vWAT), and retroperitoneal WAT was reduced in female $APP^{NL-F/NL-F}$ after D+Q treatment, but increased with Fisetin. Neither senolytic treatment effected WAT in males (Fig. 1B-E). Fisetin increased interscapular BAT in female $APP^{NL-F/NL-F}$ mice but no changes were observed in the other groups (Fig. 1F). Body weight treatment effects were largely influenced by the changes in adiposity.

The observed body composition differences could impact circulating lipids promoting dyslipidemia which increases the risk for developing cognitive impairments. Plasma triglyceride levels were decreased solely in females undergoing D+Q treatment but no changes were found in the other groups compared with control treatment (Fig. 1G). Cholesterol levels in plasma did not change with either of the treatment conditions in both the male and female mice (Fig.1H). In summary, D+Q treatment reduced WAT,

body weight, and circulating triglycerides while Fisetin treatment increased WAT, BAT, and body weight in female $APP^{NL\text{-}F/NL\text{-}F}$ mice. Neither D+Q nor Fisetin affected these measures in male $APP^{NL\text{-}F/NL\text{-}F}$ mice.

Effects of senolytic drug treatments on glucose metabolism in $APP^{NL\text{-}F/NL\text{-}F}$ mice

Adipose tissue modulates glucose homeostasis, so we assayed the effects of senolytic intervention on blood glucose levels in $APP^{NL\text{-}F/NL\text{-}F}$ mice. A glucose tolerance test (GTT) for glucose clearance and insulin tolerance test (ITT) for insulin sensitivity were performed. GTT and ITT results were unchanged regardless of sex or senolytic treatment compared with control groups (Fig. 2A-F). In female $APP^{NL\text{-}F/NL\text{-}F}$ mice, D+Q and Fisetin treatment reduced fasting glucose, while D+Q treatment lowered fed glucose levels and plasma insulin (Fig. 2G-I). Fisetin and D+Q increased male $APP^{NL\text{-}F/NL\text{-}F}$ plasma insulin levels (Fig 2I). D+Q treatment drastically reduced circulating adiponectin levels in male $APP^{NL\text{-}F/NL\text{-}F}$ mice (Fig. 2J). Despite these changes to plasma insulin and adiponectin in male $APP^{NL\text{-}F/NL\text{-}F}$ mice, no corresponding blood glucose changes were observed with the GTT or ITT (Fig. 2A,C,E-H).

Effects of senolytic drug treatments on energy expenditure in $APP^{NL\text{-}F/NL\text{-}F}$ mice

Aside from being an important regulator of glucose homeostasis, adipose tissue is also a central metabolic organ in the regulation of energy homeostasis [24]. Since D+Q and Fisetin senolytic drug treatments altered adipose tissue composition (Fig. 1A-E), indirect calorimetry was used to assess senolytic treatment effects on energy metabolism in $APP^{NL\text{-}F/NL\text{-}F}$ mice. Data revealed that D+Q treatment elevated oxygen consumption

(VO_2; Fig. 3B-C) and energy expenditure (EE; Fig. 3E-F) without affecting respiratory quotient (RQ; Fig 3H-I in the female $APP^{NL-F/NL-F}$ mice, while Fisetin elicited no effects. In contrast, neither treatment altered the energy metabolism in male $APP^{NL-F/NL-F}$ mice (Fig. 3A,C,D,F,G,I).

D+Q treatment reduces visceral white adipose tissue and hippocampal senolytic markers in female $APP^{NL-F/NL-F}$ mice

As previously discussed, D+Q and Fisetin have been reported to reduce senescent cell burden in numerous models of aging and disease [8]. Adipose tissue, specifically vWAT, contains the highest burden of senescent cells [25] and has a stronger correlation with brain atrophy than age, BMI, hypertension, or type 2 diabetes mellitus [26]. Since D+Q and Fisetin treatment altered adiposity in female $APP^{NL-F/NL-F}$ mice (albeit with contrasting effects), we further examined whether senescent cell markers and SASP were affected in vWAT. The results showed that D+Q treatment downregulated gene expression of $p16^{Ink4a}$, $p21^{Cip1}$, IL-6, TNFα, MCP1, and IL-10 within female $APP^{NL-F/NL-F}$ mice (Fig. 4A-F). In contrast, D+Q treatment in male $APP^{NL-F/NL-F}$ mice increased gene expression of $p21^{Cip1}$, IL-6, TNFα, MCP1, IL-10, MIP1α, and CXCL16 (Fig. 4B-H) in vWAT. Fisetin treatment had no effect on vWAT genes in either sex of $APP^{NL-F/NL-F}$ mice. Within the hippocampus, relative expression of $p16^{Ink4a}$, $p21^{Cip1}$, and TNFα (Fig 4I-K) were all decreased in D+Q treated female $APP^{NL-F/NL-F}$ mice, similar to vWAT. D+Q treated males also had reduced TNFα hippocampal expression, while no effects were observed in either sex after Fisetin treatment. Overall,

D+Q treatment reduced central and peripheral senescent and SASP makers in female $APP^{NL-F/NL-F}$ mice.

D+Q treatment reduces hippocampal plaque burden in female $APP^{NL-F/NL-F}$ mice

Higher senescence and SASP markers in adipose tissue was linked to cognitive deficits and increased dementia risk [27]. Accordingly, it is important to know whether the senolytic drug treatments mitigate senescence and amyloid plaques in the brain of $APP^{NL-F/NL-F}$ mice. Acidic senescence-associated-β-galactosidase (SA-β-gal) staining has been extensively used as a marker of cellular senescence *in vivo* in both whole-mount and cryosections [28]. To examine the treatment effects on cell senescence and amyloid plaques in the hippocampus, tissue was co-stained with SA-β-gal for senescence (blue) and congo red for amyloid plaques (red). The representative stained images (Fig. 5A) and quantified data showed that D+Q treatment in the female $APP^{NL-F/NL-F}$ mice reduced the percentage of SA-β-gal staining (Fig. 5B) and the plaque number, size, density, and burden throughout the hippocampus (Fig. 5C-F). Since soluble amyloid-β $(A\beta)_{42}$ is considered the neurotoxic species associated with AD development and its aggregation results in insoluble plaque deposition, we also assayed its hippocampal levels. Hippocampal soluble $A\beta_{42}$ was reduced in D+Q treated female $APP^{NL-F/NL-F}$ mice (Fig 5G). D+Q treatment in male $APP^{NL-F/NL-F}$ mice as well as Fisetin treatment in both sexes did not drastically alter hippocampal soluble or insoluble amyloid levels (Fig. 5C-G). Furthermore, a sex effect was discovered with respect to males portraying a smaller plaque size than females within the control condition (Fig. 5D),

which is consistent with our previous observations [29]. However, this sex effect did not carry over into any of the treatment groups.

D+Q treatment improved spatial learning and memory in female APP$^{NL-F/NL-F}$ mice

To examine whether senolytic treatment improves spatial learning and memory recall in APP$^{NL-F/NL-F}$ mice, the Morris water maze (MWM) test was performed after 9 months of treatments at 13 months of age. The MWM data demonstrated that D+Q treated female APP$^{NL-F/NL-F}$ mice improved spatial learning during the 5-day training period by reducing cumulative distance (Fig. 6B-C), decreasing corrected integrated path length (CIPL; Fig. 6E-F), and increasing path efficiency (Fig. 6H-I). D+Q treatment also improved spatial memory recall by significantly increasing platform entries during the probe challenge (Fig. 6J). Fisetin treatment in female APP$^{NL-F/NL-F}$ mice had minimal effects on spatial navigation, though an increase in path efficiency during the training days was observed (Fig. 6H-I). MWM spatial learning and memory recall was not altered in male APP$^{NL-F/NL-F}$ mice receiving either D+Q or Fisetin (Fig. 4A,C,D,F,G,I-J). The improved cognitive performance observed in female APP$^{NL-F/NL-F}$ may be due to the reduced SASP profile as well as soluble and insoluble amyloid accumulation.

Discussion and Conclusion:

Primary prevention using senolytics had sexually dimorphic effects in APP$^{NL-F/NL-F}$ mice. D+Q treatment in female APP$^{NL-F/NL-F}$ mice improved multiple peripheral and metabolic parameters including reduced body weight and adiposity, leading to

improvements in triglyceride, insulin, and blood glucose levels as well as enhanced energy metabolism. D+Q treatment in female $APP^{NL-F/NL-F}$ mice also decreased SASP markers in vWAT and the hippocampus. Furthermore, D+Q treatment in female $APP^{NL-F/NL-F}$ mice decreased hippocampal soluble and insoluble $A\beta_{42}$ and SA-β-gal staining. The culmination of these factors positively impacted spatial learning and memory in female $APP^{NL-F/NL-F}$ mice. In male $APP^{NL-F/NL-F}$ mice, D+Q treatment had an opposing effect whereby senescent cell markers and the SASP profile was increased while negatively impacting circulating insulin and adiponectin. Although the senescence and plasma profiles were worse, this did not alter overall body composition, blood glucose levels, energy metabolism, plaque burden, nor cognitive impairments beyond what was reported for vehicle treatment. Fisetin had negligible effects in $APP^{NL-F/NL-F}$ males while increasing adiposity in the females.

The reasons behind the sexually dimorphic responses to the senolytics used in this current study may partially be explained by an earlier onset of disease progression in female $APP^{NL-F/NL-F}$ mice. Although $APP^{NL-F/NL-F}$ mice develop cognitive impairment at 12-18 months of age [18] when hippocampal plaque accumulation is prevalent, we have previously shown females accumulate more plaques [30] and have worse cognitive deficits as they age [31] compared to males. The present study also highlighted that senescent cell markers (SA-β-gal, $p16^{Ink4a}$) as well as soluble and insoluble $A\beta_{42}$ were elevated in vehicle treated females compared to treatment matched male $APP^{NL-F/NL-F}$ mice. Senolytics clear senescent cells or reverse cellular senescence rather than preventing cells from entering a senescent state. The D+Q treatment may have been

efficacious in female $APP^{NL-F/NL-F}$ mice because the disease progression and senescent cell burden was more pronounced compared with male littermates.

The sex-dependent D+Q treatment effects in $APP^{NL-F/NL-F}$ mice could also be attributed to differences in adiposity and adiponectin. Although D+Q treatment in the male $APP^{NL-F/NL-F}$ mice did not change body weight nor WAT accumulation, the treatment drastically reduced circulating levels of adiponectin, which has strong anti-inflammatory properties [32, 33]. The decreased adiponectin in D+Q treated male $APP^{NL-F/NL-F}$ mice could have led to the increase in vWAT SASP. However, elevated peripheral inflammation in the male mice treated with D+Q did not affect hippocampal inflammatory senolytic markers, plaque burden, or cognitive function. Although adiponectin levels were unchanged after senolytic intervention in female $APP^{NL-F/NL-F}$ mice, D+Q treatment reduced body weight, WAT depots, and vWAT senescent cell markers along with the SASP profile.

Metabolic changes also underlie the differential sex responses to senolytic intervention. Besides reduced adiposity, D+Q treated female $APP^{NL-F/NL-F}$ mice had improved energy metabolism potentially contributing to the lower plasma insulin and basal blood glucose levels. Circulating triglyceride levels, associated with a lower AD risk in women [34], were also decreased. Both senolytic treatments increased plasma insulin levels in male $APP^{NL-F/NL-F}$ mice, suggesting impaired glucose utilization, although this was not observed with the ITT or GTT. We suspect that there may be more factors

involved in the sex-dependent response of $APP^{NL-F/NL-F}$ mice to the senolytic drugs used in the current study, which warrants further investigation.

$APP^{NL-F/NL-F}$ mice are backcrossed onto a C57BL/6 background strain. Surprisingly, these results contrast with our previous studies utilizing a similar experimental paradigm in C57BL/6 mice [20]. We previously demonstrated that D+Q treatment elevated SASP expression, increased WAT mass, and reduced energy metabolism that decreased cognitive performance in female C57BL/6 mice. The dichotomous results between these two studies may be attributed to factors associated with physiological and pathological aging. Unlike during physiological aging in C57BL/6 mice, the APP knock-in pathologically predisposes mice to amyloid accumulation that drives production of neuroinflammation and induces senescence [35]. Surprisingly, D+Q treatment in male $APP^{NL-F/NL-F}$ mice increased vWAT inflammatory markers. While the mechanisms behind this remain to be elucidated, detrimental effects of D+Q administration are not unique to this study. Using the same dosing concentration, D+Q treatment worsened male hepatocellular carcinoma in male C57BL/6 mice [36]. Others have proposed that continuous senescent cell removal beginning at young ages does not always activate regenerative processes, but rather causes fibrosis that is detrimental to the healthspan of the organism [37].

Previous reports support a role for estrogen in reducing or preventing cognitive decline [38], potentially through a mechanism whereby estradiol reduces amyloid plaques by preferentially increasing APPα over APPβ [39, 40]. In a separate study, D+Q treatment has been shown to overcome negative effects of estrogen-deficiency, such as

postmenopausal osteoporosis [41]. We previously discussed a possibility of D+Q treatment leading to low estrogen levels in normal aging C57BL/6 mice [20], however, data support the sometimes contradictory differential effects of early intervention between normal aging and mouse models of AD [31]. This, combined with the general lack of characterization of estrogen levels across disease progression in $APP^{NL\text{-}F/NL\text{-}F}$ mice, makes it difficult to determine if the effects of D+Q treatment in $APP^{NL\text{-}F/NL\text{-}F}$ mice are mediated through modulating estrogen levels. Based on the current study, future experiments to address this gap in knowledge are warranted.

A couple of study design limitations should be noted. First was an inability to conduct the *in vivo* assays during a single treatment window. The duration needed to complete the metabolic and cognitive assays required these parameters to be assayed across several months as to avoid confounds due to testing during senotherapeutic dosing weeks. The lack of effects seen on energy metabolism or glucose regulation despite worse circulating concentrations of insulin and adiponectin may be due to fewer senolytic treatments received. However, the trends towards D+Q benefits in females and detriments in males were consistent across the assays. Second, we tested the senolytics in young mice to determine their efficacy as a primary interventional strategy. It is possible the compounds may have different therapeutic effects at different stages of disease progression.

Overall, our current study shows that administering D+Q during a primary prevention window reduced central and peripheral markers of senescence and SASP in female

$APP^{NL-F/NL-F}$ mice. This led to improvements in adiposity, metabolism, and cognitive performance. Considering women have a greater risk of developing dementia during their lifetime, identifying senotherapeutics appropriate for sex and dementia stage is necessary for personalized AD therapies [42].

Materials and methods

Chemicals

Unless otherwise noted, all chemicals were obtained from Sigma-Aldrich (St. Louis, MO) including Quercetin (Cat# RHR1488). Fisetin was purchased from Selleckchem (Houston, TX; Cat #S2298), and Dasatinib from LC laboratories (Woburn, MA; Cat# D-3307).

Animals

$APP^{NL-F/NL-F}$ mice on a C57BL/6 background (RRID: IMSR_RBRC06343) were obtained from Riken (Japan). Protocols for animal use were approved by the *Institutional Animal Care and Use Committee* at Southern Illinois University School of Medicine (Protocol number: 2022-055), which is accredited by the Association for Assessment and Accreditation of Laboratory Animal Care. Mice were group housed on a 12:12 h light-dark cycle, with food (Chow 5001 with 23.4% protein, 5% fat, and 5.8% crude fiber; LabDiet PMI Feeds) and water available *ad libitum*. The majority of experiments were conducted during the light phase except for indirect calorimetry where data was obtained for a 24 hr cycle. Genotypes were confirmed by collecting a 5 mm tail tip for DNA analysis by TransnetYX, Inc (Cordova, TN).

Senolytic treatment

Senotherapeutic concentrations and dosing strategy were based on previous publications [20, 43, 45]. $APP^{NL-F/NL-F}$ mice were dosed with 100 mg/kg of Fisetin while a cocktail of 5 mg/kg of D + 50 mg/kg of Q, or vehicle (2% DMSO in canola oil) by oral administration [45]. The treatments were given once per month from 4-13 months of age. All assays, including tissue collection, were conducted one week after monthly senotherapeutic dosing. The dosing strategy was based on previous literature showing that markers of cell senescence are still reduced after a four week off-treatment period [8]. Since senescent cell accumulation occurs over weeks, maintaining an effective concentration dosage is not required. Rather, intermittent dosing may be preferable thereby avoiding adverse effects.

Body composition and tissue procurement

A week following the final senotherapeutic treatment at 13 months of age, body weight was recorded and mice were sedated using isoflurane. A cardiac puncture was used to collect the plasma. Mice were rapidly decapitated and the peripheral tissues (liver, heart, kidney, pancreas, spleen, WAT, and BAT) were weighed to calculate their contribution to total body weight. Tissue was immediately flash frozen and stored at -80˚C until processing as previously described [20].

Glucose tolerance test (GTT) and insulin tolerance test (ITT)

Glucose metabolism was assessed via GTT and ITT after six treatments at the animal age of nine months as previously described [20]. Fifteen-hour-fasted mice underwent

GTT by intraperitoneal (i.p.) injection with 1 g glucose per kg of body weight (BW). Blood glucose levels were measured at 0, 15, 30, 45, 60, and 120 min with a PRESTO glucometer (AgaMatrix). For ITT, nonfasted mice were injected i.p. with 1 IU porcine insulin from sigma (St. Louis, MO) (Cat# I5523) per kg of BW. Blood glucose levels were measured at 0, 15, 30, 45, 60, and 120 min. The data for GTT and ITT is presented as absolute value.

Indirect calorimetry

Energy metabolism was measured by indirect calorimetry at the animal age of twelve months using an AccuScan Metabolic System (AccuScan Instruments). In this system, mice are housed individually in metabolic chambers with *ad libitum* access to food and water. After a twenty-four-hour acclimation period, VO_2, VCO_2, EE, and RQ measurements were collected every ten minutes per animal and averaged for each hour.

Soluble $A\beta_{42}$ Determination

The hippocampus from one hemisphere was dissected and stored at -80°C until tissue processing. Soluble $A\beta_{42}$ concentrations were determined using the Human / Rat β amyloid ELISA kits (WAKO Chemicals; Cat: 292-64501) according to the manufacturer recommended protocols.

Hippocampal amyloid plaque and acidic senescence-associated-β-galactosidase (SA-β-gal) staining and quantification.

Immediately following dissection, hemibrains were fixed in 4% paraformaldehyde then transferred into 30% sucrose in 0.1M phosphate buffer prior to cryosectioning [46]. Twenty micron coronal sections through the hippocampus were obtained and every sixth serial section was stained for senescent cells and amyloid plaques. Free floating slices were stained for SA-β-gal per the manufacturer's protocol (Cell Signaling Technology Danvers, MA, Cat#9860). Each slice was rinsed with 1X PBS then transferred to 1X Fixative Solution for 10-15 minutes followed by rinsing twice with 1X PBS. Slices were placed in β-gal staining solution (pH=6.0) and incubated for ~18 hrs at 37°C. Following overnight incubation, slices were rinsed in 1X PBS, then mounted onto subbed microslides and allowed to dry before staining for amyloid plaques with 1% Congo Red (1 hr) according to the methods of Rajamohamedsait and Sigurdsson, 2012 [47]. After staining, slides were dehydrated using increasing concentrations of ethanol followed by submersion in CitriSolv for 5-10 min then immediately cover slipped using Permount (Fisher Scientific, Cat# SP15-500). Samples were imaged in brightfield at 4x and 40x magnification using a Keyence BZ-X810 All-in-One Fluorescence Microscope and accompanying analysis software (Keyence Corp.). The hippocampus was manually outlined and regions of interest were extracted by hue for each stain using the software's Hybrid Cell Count function that determined plaque number and size, as well as the area of the hippocampus, plaques, and SA-β-gal stained regions. Senescence and plaque burden were calculated as a percentage of SA-β-gal-stained area within the hippocampus for each sample [48, 49]. Verification and quantification of amyloid plaques was conducted according to our previous protocols [29].

Four hippocampal slices were averaged to obtain an individual sample for each mouse.

Morris water maze (MWM) training and probe challenge

The MWM was used to assess spatial learning and memory recall, and performed as previously described [50]. In short, mice were trained to utilize visual cues placed around the room to repeatedly swim to a static, hidden escape platform (submerged one cm below the opaque water surface), regardless of starting quadrant. The MWM paradigm consisted of 5 consecutive training days with three, 90 s trials/day and a minimum inter-trial-interval of 20 min. Starting quadrant was randomized for each trial. After two days without testing, the escape platform was removed and all mice entered the pool of water from the same starting position for a single 60 s probe challenge to test long-term memory recall. The ANY-maze video tracking system (Stoelting Co., Wood Dale, IL) was used to record mouse navigation during the training and probe challenge. The three trials for each training day were averaged for each mouse.

Assessment of blood chemistry

Plasma was collected from animals anesthetized with isoflurane by cardiac puncture at the time of sacrifice. The blood was mixed with EDTA, followed by centrifugation at 10,000 g for 15 min at 4°C for plasma collection. Plasma was frozen at -80˚C until determination of insulin and adiponectin (Crystal Chem, Elk Grove Village, IL; Cat# 90080 and 80569) by ELISA. Triglycerides or cholesterol (Pointe Scientific, Canton, MI; Cat# T7532-120 and C7510-120) was measured using the manufacturers' recommended protocols.

RT–PCR

mRNA expression was analyzed by quantitative RT–PCR as previously described using cDNA synthesis kits and SYBR green mix from Bio-Rad (Cat# 1708897 and 1725121) performed with the StepOne Real-Time PCR System (Thermo Fisher Scientific) or the QuantStudio PCR System (Applied Biosystems). RNA was extracted using RNeasy mini kits or RNeasy Lipid Tissue Mini Kits (Qiagen) following the manufacturer's instructions. Relative expression was calculated as previously described [51] and primers were purchased from Integrated DNA Technologies. The housekeeping genes glyceraldehyde 3-phosphate dehydrogenase (GAPDH) was used for adipose tissue while ubiquitin conjugating enzyme E2 D2 (UBE2D2) was used for the hippocampus. A list of forward and reverse primers is shown in Table 1.

Statistical analysis

Statistical analyses were conducted using a two-way ANOVA to test for significance of sex (males × females), treatment (Vehicle × Fisetin or D+Q), and interaction effects (sex x treatment). Differences between vehicle and senolytic treatments were determined with unpaired two-tailed Student's t tests with significance defined as $p \leq 0.05$. Data are presented as means ± SEM. All statistical analyses and graphs were completed using Prism 10 (GraphPad Inc, La Jolla, CA, USA).

Acknowledgements

This work was supported by the National Institutes of Health NIA R01-AG057767 and NIA R01-AG061937, Kenneth Stark Endowment, and Dale and Deborah Smith Center

for Alzheimer's Research and Treatment (YF, MRP, KQ, SM, SR, KNH, ERH).

Geriatrics Initiative (DM, AB).

Author Contributions:

YF, MRP, KQ, SM, and DM conducted the experiments and analyzed the data. YF, AB, KNH, and ERH conceived the study, designed the experiments, interpreted the data, and wrote the manuscript. SR assisted with manuscript editing. All authors approved the final version of the manuscript.

Statement and Declarations

The authors state that they have no financial or non-financial competing interests to disclose.

Data Availability

All data is available upon reasonable request.

References

1. Musiek, E.S., T. Gomez-Isla, and D.M. Holtzman, *Aducanumab for Alzheimer disease: the amyloid hypothesis moves from bench to bedside.* J Clin Invest, 2021. **131**(20).
2. Hardy, J.A. and G.A. Higgins, *Alzheimer's disease: the amyloid cascade hypothesis.* Science, 1992. **256**(5054): p. 184-5.
3. Kametani, F. and M. Hasegawa, *Reconsideration of Amyloid Hypothesis and Tau Hypothesis in Alzheimer's Disease.* Front Neurosci, 2018. **12**: p. 25.
4. Gonzales, M.M., et al., *Senolytic Therapy to Modulate the Progression of Alzheimer's Disease (SToMP-AD): A Pilot Clinical Trial.* J Prev Alzheimers Dis, 2022. **9**(1): p. 22-29.
5. Breijyeh, Z. and R. Karaman, *Comprehensive Review on Alzheimer's Disease: Causes and Treatment.* Molecules, 2020. **25**(24).
6. Guerreiro, R. and J. Bras, *The age factor in Alzheimer's disease.* Genome Med, 2015. **7**: p. 106.
7. Hascup, E.R. and K.N. Hascup, *Toward refining Alzheimer's disease into overlapping subgroups.* Alzheimers Dement (N Y), 2020. **6**(1): p. e12070.
8. Kirkland, J.L. and T. Tchkonia, *Senolytic drugs: from discovery to translation.* J Intern Med, 2020. **288**(5): p. 518-536.
9. van Deursen, J.M., *The role of senescent cells in ageing.* Nature, 2014. **509**(7501): p. 439-46.
10. Baker, D.J. and R.C. Petersen, *Cellular senescence in brain aging and neurodegenerative diseases: evidence and perspectives.* J Clin Invest, 2018. **128**(4): p. 1208-1216.
11. Campisi, J., *Senescent cells, tumor suppression, and organismal aging: good citizens, bad neighbors.* Cell, 2005. **120**(4): p. 513-22.
12. Ohtani, N., *The roles and mechanisms of senescence-associated secretory phenotype (SASP): can it be controlled by senolysis?* Inflamm Regen, 2022. **42**(1): p. 11.
13. Bussian, T.J., et al., *Clearance of senescent glial cells prevents tau-dependent pathology and cognitive decline.* Nature, 2018. **562**(7728): p. 578-582.
14. Musi, N., et al., *Tau protein aggregation is associated with cellular senescence in the brain.* Aging Cell, 2018. **17**(6): p. e12840.
15. Zhang, P., et al., *Senolytic therapy alleviates Abeta-associated oligodendrocyte progenitor cell senescence and cognitive deficits in an Alzheimer's disease model.* Nat Neurosci, 2019. **22**(5): p. 719-728.
16. Wang, D.M., et al., *Effects of long-term treatment with quercetin on cognition and mitochondrial function in a mouse model of Alzheimer's disease.* Neurochem Res, 2014. **39**(8): p. 1533-43.
17. Sabogal-Guaqueta, A.M., et al., *The flavonoid quercetin ameliorates Alzheimer's disease pathology and protects cognitive and emotional function in aged triple transgenic Alzheimer's disease model mice.* Neuropharmacology, 2015. **93**: p. 134-45.
18. Saito, T., et al., *Single App knock-in mouse models of Alzheimer's disease.* Nat Neurosci, 2014. **17**(5): p. 661-3.

19. Benitez, D.P., et al., *Knock-in models related to Alzheimer's disease: synaptic transmission, plaques and the role of microglia.* Mol Neurodegener, 2021. **16**(1): p. 47.
20. Fang, Y., et al., *Sexual dimorphic metabolic and cognitive responses of C57BL/6 mice to Fisetin or Dasatinib and quercetin cocktail oral treatment.* Geroscience, 2023. **45**(5): p. 2835-2850.
21. Perry, G., et al., *Oxidative damage in Alzheimer's disease: the metabolic dimension.* Int J Dev Neurosci, 2000. **18**(4-5): p. 417-21.
22. Schmitt, K., et al., *Insights into mitochondrial dysfunction: aging, amyloid-beta, and tau-A deleterious trio.* Antioxid Redox Signal, 2012. **16**(12): p. 1456-66.
23. Yao, J., et al., *Mitochondrial bioenergetic deficit precedes Alzheimer's pathology in female mouse model of Alzheimer's disease.* Proc Natl Acad Sci U S A, 2009. **106**(34): p. 14670-5.
24. Choe, S.S., et al., *Adipose Tissue Remodeling: Its Role in Energy Metabolism and Metabolic Disorders.* Front Endocrinol (Lausanne), 2016. **7**: p. 30.
25. Palmer, A.K., T. Tchkonia, and J.L. Kirkland, *Senolytics: Potential for Alleviating Diabetes and Its Complications.* Endocrinology, 2021. **162**(8).
26. Lake, J.E., et al., *Visceral fat is associated with brain structure independent of human immunodeficiency virus infection status.* J Neurovirol, 2017. **23**(3): p. 385-393.
27. Moser, V.A. and C.J. Pike, *Obesity and sex interact in the regulation of Alzheimer's disease.* Neurosci Biobehav Rev, 2016. **67**: p. 102-18.
28. Dimri, G.P., et al., *A biomarker that identifies senescent human cells in culture and in aging skin in vivo.* Proc Natl Acad Sci U S A, 1995. **92**(20): p. 9363-7.
29. McFadden, S., et al., *Chronic, Mild Hypothermic Environmental Temperature Does Not Ameliorate Cognitive Deficits in an Alzheimer's Disease Mouse.* J Gerontol A Biol Sci Med Sci, 2023. **78**(6): p. 911-919.
30. Britz, J., et al., *Assessing Sex-Specific Circadian, Metabolic, and Cognitive Phenotypes in the AbetaPP/PS1 and APPNL-F/NL-F Models of Alzheimer's Disease.* J Alzheimers Dis, 2022. **85**(3): p. 1077-1093.
31. Findley, C.A., et al., *Prodromal Glutamatergic Modulation with Riluzole Impacts Glucose Homeostasis and Spatial Cognition in Alzheimer's Disease Mice.* J Alzheimers Dis, 2023. **94**(1): p. 371-392.
32. Ouchi, N. and K. Walsh, *Adiponectin as an anti-inflammatory factor.* Clin Chim Acta, 2007. **380**(1-2): p. 24-30.
33. Ter Horst, R., et al., *Sex-Specific Regulation of Inflammation and Metabolic Syndrome in Obesity.* Arterioscler Thromb Vasc Biol, 2020. **40**(7): p. 1787-1800.
34. Ancelin, M.L., et al., *Sex differences in the associations between lipid levels and incident dementia.* J Alzheimers Dis, 2013. **34**(2): p. 519-28.
35. Walton, C.C., et al., *Senescence as an Amyloid Cascade: The Amyloid Senescence Hypothesis.* Front Cell Neurosci, 2020. **14**: p. 129.

Abbreviations: Alzheimer's disease (AD), Amyloid beta (Aβ), area under the curve (AUC), body weight (bw), brown adipose tissue (BAT), carbon dioxide consumption (VCO_2), corrected integrated path length (CIPL), Dasatinib (D), energy expenditure (EE), glucose tolerance test (GTT), insulin tolerance test (ITT), intraperitoneal (i.p.), Morris water maze (MWM), oxygen consumption (VO_2), Quercetin (Q), respiratory quotient (RQ), senescence-associated-β-galactosidase (SA-β-gal), senescence associated secretory phenotype (SASP), standard error of the mean (SEM), white adipose tissue (WAT), visceral white adipose tissue (vWAT)

36. Raffaele, M., et al., *Mild exacerbation of obesity- and age-dependent liver disease progression by senolytic cocktail dasatinib + quercetin.* Cell Commun Signal, 2021. **19**(1): p. 44.
37. Grosse, L., et al., *Defined p16(High) Senescent Cell Types Are Indispensable for Mouse Healthspan.* Cell Metab, 2020. **32**(1): p. 87-99 e6.
38. Rountree, S.D., et al., *Factors that influence survival in a probable Alzheimer disease cohort.* Alzheimers Res Ther, 2012. **4**(3): p. 16.
39. Manthey, D., et al., *Estrogen induces a rapid secretion of amyloid beta precursor protein via the mitogen-activated protein kinase pathway.* Eur J Biochem, 2001. **268**(15): p. 4285-91.
40. Zhang, S., et al., *Estrogen stimulates release of secreted amyloid precursor protein from primary rat cortical neurons via protein kinase C pathway.* Acta Pharmacol Sin, 2005. **26**(2): p. 171-6.
41. Wang, Y., et al., *Repurpose dasatinib and quercetin: Targeting senescent cells ameliorates postmenopausal osteoporosis and rejuvenates bone regeneration.* Bioact Mater, 2023. **25**: p. 13-28.
42. Nebel, R.A., et al., *Understanding the impact of sex and gender in Alzheimer's disease: A call to action.* Alzheimers Dement, 2018. **14**(9): p. 1171-1183.
43. Yousefzadeh, M.J., et al., *Fisetin is a senotherapeutic that extends health and lifespan.* EBioMedicine, 2018. **36**: p. 18-28.
44. Palmer, A.K., et al., *Targeting senescent cells alleviates obesity-induced metabolic dysfunction.* Aging Cell, 2019. **18**(3): p. e12950.
45. Hascup, K.N. and E.R. Hascup, *Soluble Amyloid-beta42 Stimulates Glutamate Release through Activation of the alpha7 Nicotinic Acetylcholine Receptor.* J Alzheimers Dis, 2016. **53**(1): p. 337-47.
46. Rajamohamedsait, H.B. and E.M. Sigurdsson, *Histological staining of amyloid and pre-amyloid peptides and proteins in mouse tissue.* Methods Mol Biol, 2012. **849**: p. 411-24.
47. Liu, P., et al., *Quantitative Comparisons of Large Numbers of Human Plasma Samples Using TMT10plex Labeling.* Methods Mol Biol, 2017. **1619**: p. 319-337.
48. Hayes, C.D., et al., *Striking reduction of amyloid plaque burden in an Alzheimer's mouse model after chronic administration of carmustine.* BMC Med, 2013. **11**: p. 81.
49. Hascup, K.N., et al., *Hippocampal alterations in glutamatergic signaling during amyloid progression in AbetaPP/PS1 mice.* Sci Rep, 2020. **10**(1): p. 14503.
50. Masternak, M.M., et al., *Metabolic effects of intra-abdominal fat in GHRKO mice.* Aging Cell, 2012. **11**(1): p. 73-81.

Abbreviations: Alzheimer's disease (AD), Amyloid beta (Aβ), area under the curve (AUC), body weight (bw), brown adipose tissue (BAT), carbon dioxide consumption (VCO_2), corrected integrated path length (CIPL), Dasatinib (D), energy expenditure (EE), glucose tolerance test (GTT), insulin tolerance test (ITT), intraperitoneal (i.p.), Morris water maze (MWM), oxygen consumption (VO_2), Quercetin (Q), respiratory quotient (RQ), senescence-associated-β-galactosidase (SA-β-gal), senescence associated secretory phenotype (SASP), standard error of the mean (SEM), white adipose tissue (WAT), visceral white adipose tissue (vWAT)

Figure Legends

Figure 1 – Senolytic intervention reduced adiposity and circulating lipid levels in female APP$^{NL-F/NL-F}$ mice. Mouse body weight (A) along with percentages of total (B), WAT depots (C-E), and BAT (F) in relation to body weight. Plasma triglyceride and cholesterol levels were determined by enzymatic determination (G-H). All tissue was collected at the time of euthanization (14 months of age). Data are represented as means ± SEM (n=15-21). Results of a two factorial analysis are shown above each bar graph for the Sex (S) and Treatment (T) categorial variables and their interaction (S x T). *p<0.05, **p<0.01, ***p<0.001 based on a two-tailed Student's *t* test.

Figure 2 – Blood glucose and plasma insulin are improved after senolytic treatment in female APP$^{NL-F/NL-F}$ mice. Glucose tolerance test (GTT) and insulin tolerance test (ITT), and their respective area under the curve (AUC) after five treatments (A-F). Fasting (G) and fed (H) blood glucose levels were determined from time=0 during the GTT and ITT, respectively. Circulating insulin and adiponectin levels were determined by ELISA from plasma collected at the time of euthanization (10 treatments). Data are represented as means ± SEM (n=13-23). Results of a two factorial analysis are shown above each bar graph for the Sex (S) and Treatment (T) categorial variables and their interaction (S x T). *p<0.05, **p<0.01, ****p<0.0001 based on a two-tailed Student's *t* test.

Figure 3 – D+Q treatment improves Oxygen Consumption and energy expenditure in Female APP$^{NL-F/NL-F}$ mice. Twenty-four hour male and female oxygen consumption (A-C), energy expenditure (D-F), and respiratory quotient (G-I; VCO_2/VO_2) along with their corresponding AUC after 9 treatments were determined by indirect calorimetry. White and black bars along the abscissa indicates the hours of lights on or off, respectively. Data are represented as means ± SEM (n=15-23). Results of a two factorial analysis are shown above each bar graph for the Sex (S) and Treatment (T) categorial variables and their interaction (S x T). *p<0.05 based on a two-tailed Student's *t* test.

Figure 4 – D+Q treatment altered senescent cell markers and SASP profile in a sexually dimorphic manner. Gene expression profiles in vWAT (A-H) and the hippocampus (I-K). Data are represented as means ± SEM (n=8-10). Results of a two factorial analysis are shown above each bar graph for the Sex (S) and Treatment (T) categorial variables and their interaction (S x T). *p<0.05, **p<0.01 based on a two-tailed Student's *t* test.

Figure 5 – APP$^{NL-F/NL-F}$ mice have reduced hippocampal senescent cell burden as well as insoluble and soluble Aβ_{42} after D+Q treatment. Representative 4x and 40x hippocampal images (A) of SA-β-gal staining (blue) and plaque accumulation (red) for male (left) and female (right) after 10 treatments of vehicle (top), D+Q (middle), or Fisetin (bottom). Arrows indicate magnified image area shown to the right of each whole hippocampal image. Percentage of SA-β-gal staining (B) along with soluble (C-F) and

soluble $A\beta_{42}$ (G) levels are shown. Data are represented as means ± SEM (n=8-10). Results of a two factorial analysis are shown above each bar graph for the Sex (S) and Treatment (T) categorial variables and their interaction (S x T). *p<0.05, **p<0.01 based on a two-tailed Student's t test.

Figure 6 – Spatial learning and memory recall was improved in female $APP^{NL-F/NL-F}$ mice receiving D+Q treatment. An eight day MWM paradigm consisting of 5 training days followed by a single probe challenge 48 hrs after was used to assess spatial cognition after the eighth treatment (12 months of age). The cumulative distance (A-C), corrected integrated path length (CIPL; D-F), and path efficiency (G-I) along with their corresponding AUC are shown for each training day. The number of platform crosses into the former location of the hidden escape platform is reported for the probe challenge (J). Data are represented as means ± SEM (n=20-25). Results of a two factorial analysis are shown above each bar graph for the Sex (S) and Treatment (T) categorial variables and their interaction (S x T). *p<0.05 based on a two-tailed Student's *t* test.

Table 1 – A list of forward and reverse primers used in these studies.

Gene	Forward	Reverse
$P16^{Ink4\alpha}$	5'-CGGTCGTACCCCGATTCAG-3'	5'-GCACCGTAGTTGAGCAGAAGAG-3'
$P21^{Cip1}$	5'-CCTGGTGATGTCCGACCTG-3'	5'-CCATGAGCGCATCGCAATC-3'
IL-6	5'-CTGCAAGAGACTTCCATCCAG-3'	5'-AGTGGTATAGACAGGTCTGTTGG-3'
TNFα	5'-CAGCCGGTGCCTATGTCTC-3'	5'-CGATCACCCCGAAGTTCAGTAG-3'
MCP1	5'-CCACTCACCTGCTGCTACTCAT-3'	5'-TGGTGATCCTCTTGTAGCTCTCC-3'
IL-10	5'-GCTCTTACTGACTGGCATGAG-3'	5'-CGCAGCTCTAGGAGCATGTG-3'
MIP1α	5'-TTCTCTGTACCATGACACTCTGC-3'	5'-CGTGGAATCTTCCGGCTGTAG-3'
CXCL16	5'-CCTTGTCTCTTGCGTTCTTCC-3'	5'-TCCAAAGTACCCTGCGGTATC-3'
GAPDH	5'-AGGTCGGTGTGAACGGATTTG-3'	5'-TGTAGACCATGTAGTTGAGGTCA-3'
UBE2D2	5’-TGCCTGAGATTGCTCGGATCT-3’	5’-TCGCATACTTCTGAGTCCATTCC-3’

Figure 1: Body composition and circulating lipids after senolytic treatment.

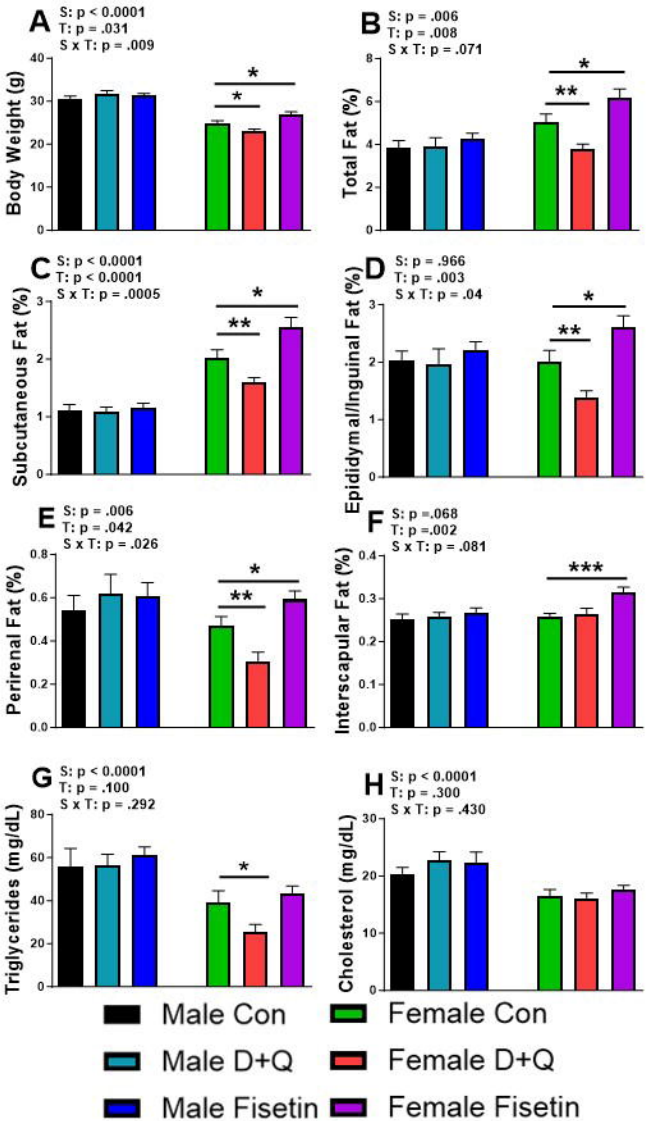

Figure 2: Senolytic effects on blood glucose, insulin, adiponectin, and triglyceride levels.

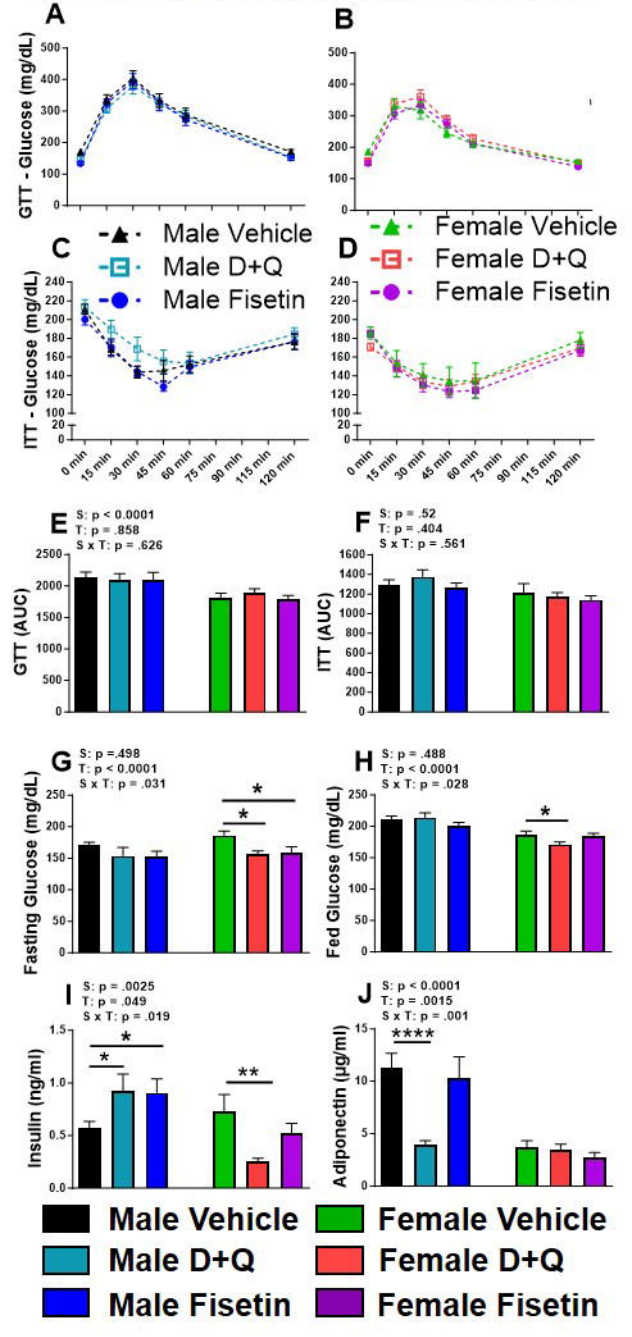

Figure 3: Senolytic effects on energy metabolism.

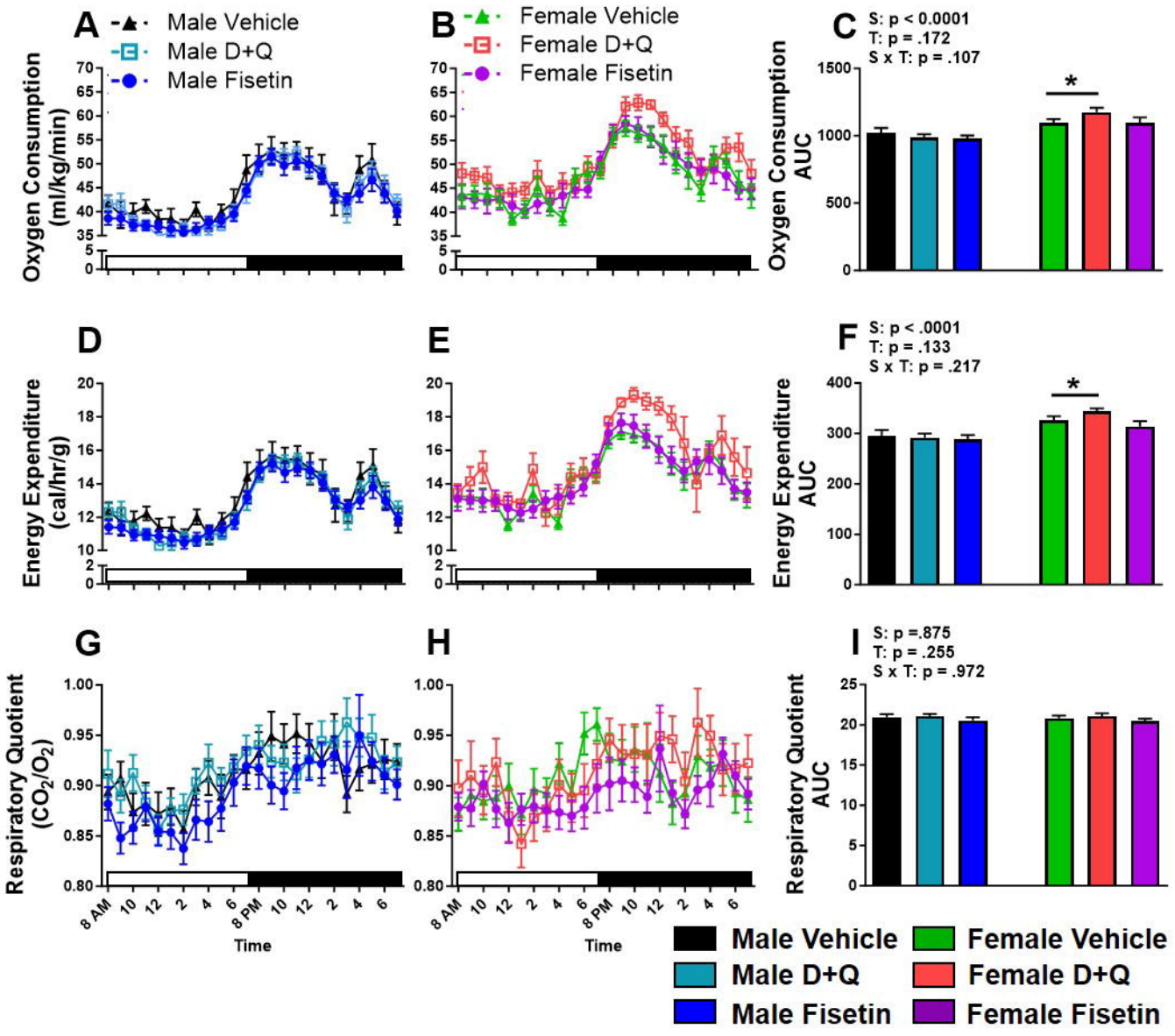

Figure 4: Relative expression of senescent cell and SASP markers in visceral adipose and hippocampal tissue.

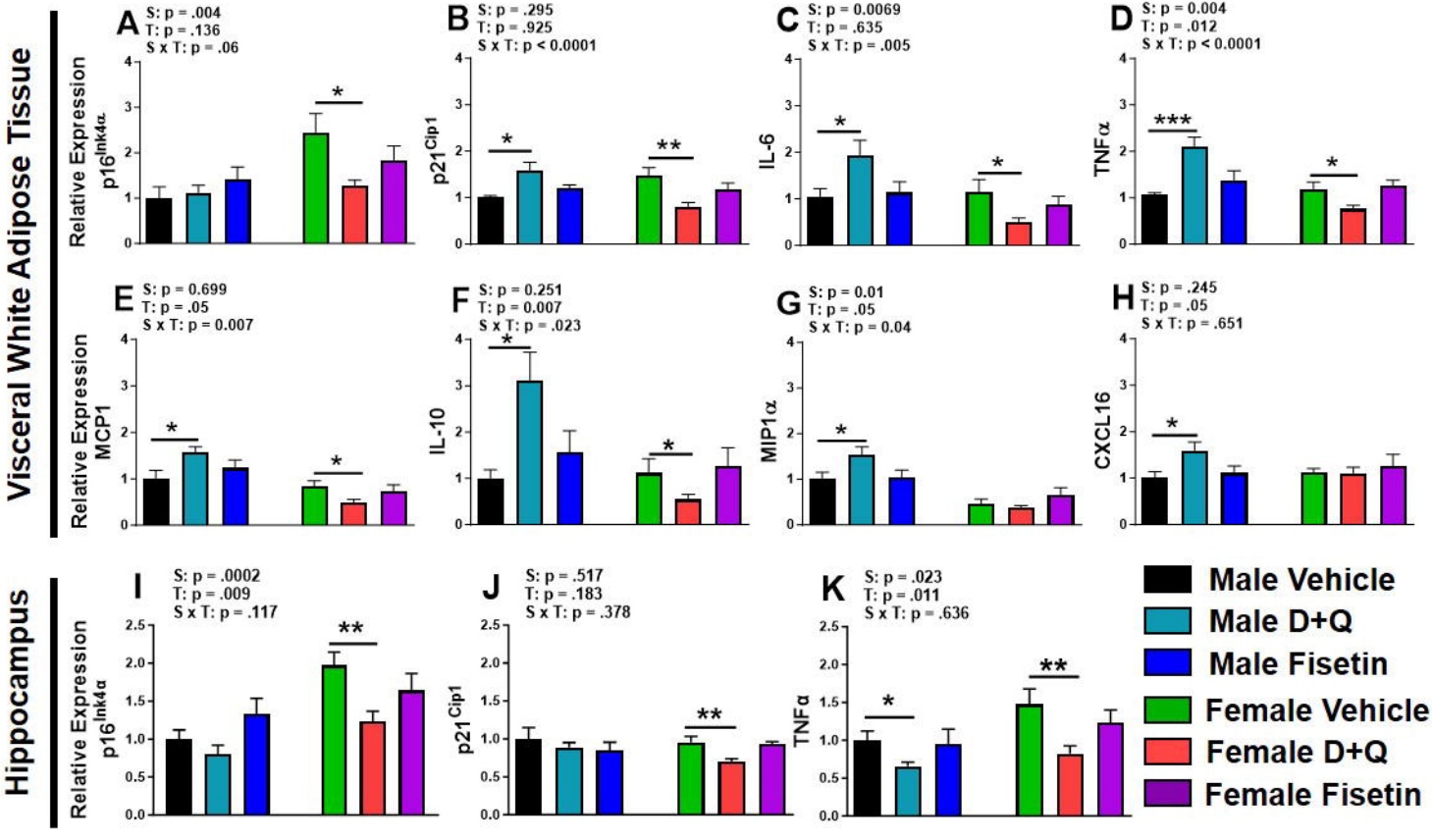

Figure 5: Hippocampal staining of SA-β-Gal and amyloid plaques as well as soluble $A\beta_{42}$ levels.

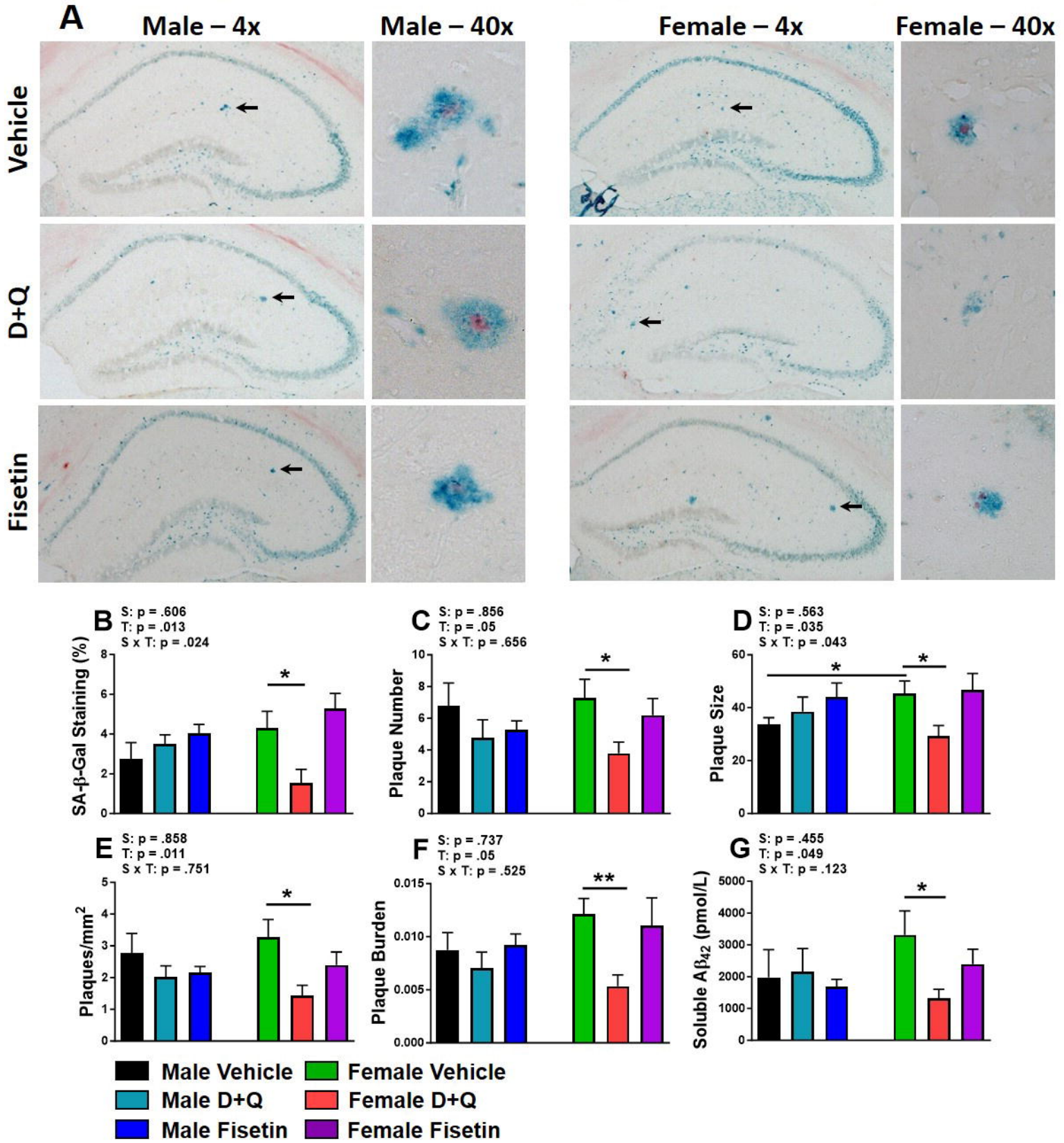
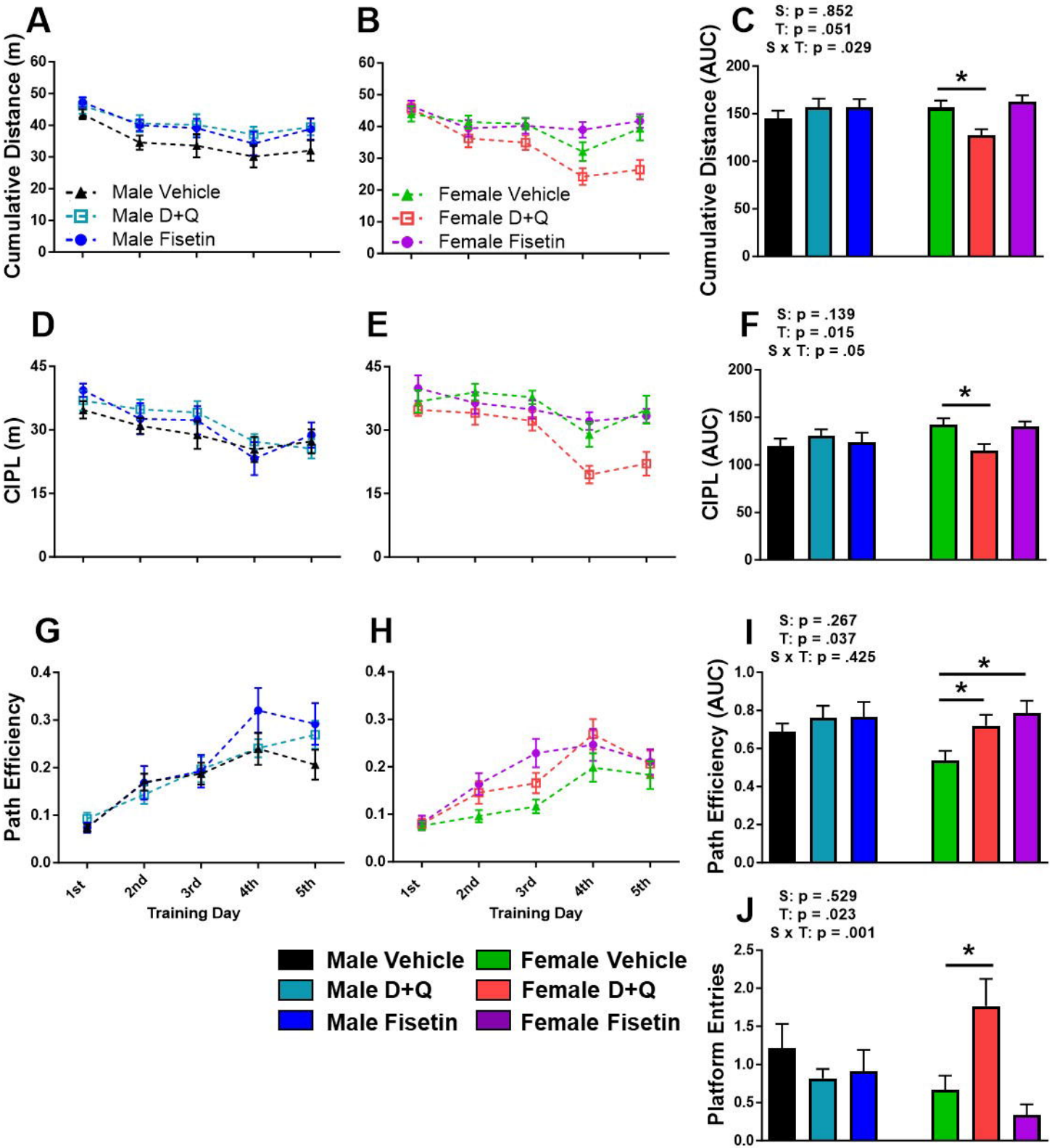
Figure 6: Senolytic treatment on spatial learning and memory recall.